ACS OMEGA

Open Access

This article is licensed under CC-BY-NC-ND 4.0

http://pubs.acs.org/journal/acsodf

Article

Nitrogen-Doped Graphene-Supported Nickel Nanoparticles Reveal Low Dehydrogenation Temperature and Long Cyclic Life of Magnesium Hydrides

Imran Muhammad, Jaffer Saddique, Chengzhang Wu, Muneeb ur Rahman, Zaheen Ullah Khan, Wajid Ali,* and Rong Zhang*

Cite This: *ACS Omega* 2024, 9, 19261−19271

Read Online

ACCESS | Metrics & More | Article Recommendations | Supporting Information

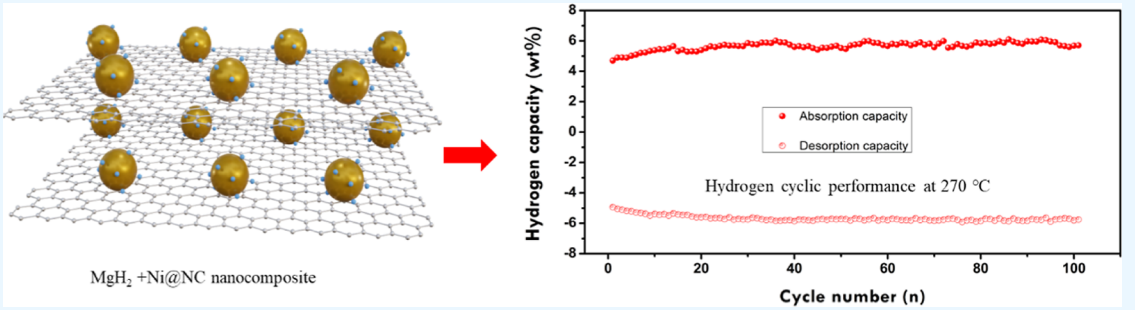

ABSTRACT: Magnesium hydride (MgH_2) is a promising hydrogen storage candidate due to its large capacity; however, high dehydrogenation temperature and slow kinetic rates are the main bottlenecks. Herein, we proposed a strategy for designing nitrogen-doped graphene-supported Ni nanoparticles (NPs) (Ni@NC) to tackle these problems. The results showed that the MgH_2 + 15 wt % Ni@NC nanocomposite reduced the on-set dehydrogenation temperature to 195 °C, which was 175 °C lower than pristine MgH_2. In addition, MgH_2 + 15 wt % Ni@NC achieved 1.7 and 6.5 wt % desorption capacities at 225 and 300 °C, respectively, while absorbing 5.5 wt % hydrogen at 100 °C. The MgH_2 + 15 wt % Ni@NC nanocomposite showed high cyclic stability, achieving 98.0% capacity retention after 100 cycles at 270 °C with negligible loss in capacity. This remarkable hydrogen storage performance can be attributed to the homogeneous distribution of Ni NPs on N-doped graphene layers, in situ formed Mg_2NiH_2 NPs, and multiphasic regions, promoting the nucleation and growth process during hydrogenation/dehydrogenation, which stabilized and improved the cyclic stability. This strategy paves the way to developing high-performance MgH_2 for large-scale applications.

INTRODUCTION

Hydrogen is a promising energy carrier, achieved from renewable resources, and exists in a wide range of varieties.[1] Hydrogen is facing the challenge of finding a suitable method for storing that can be safe, affordable, effective, and lightweight.[2−4] Compared to traditional hydrogen storage methods such as high-pressure tanks and liquid storage, magnesium hydrides (MgH_2) have attracted much attention due to their high hydrogen capacity (7.6 wt %), high reversibility, availability in nature, and low cost. Nevertheless, the practical applications of MgH_2 are obstructed by high thermodynamic stability and slow hydrogen absorption/desorption kinetic rates.[4−8]

Many researchers adopted numerous approaches such as preparing nanosized MgH_2, employing new techniques, and adding catalysts to address the mentioned-above key problems. In fact, adding catalysts is one of the efficient methods which can significantly improve the hydrogen storage performance of MgH_2. It has been reported that transition-metal oxides such as TiO_2 reduced the on-set dehydrogenation temperature lower to 145 °C than undoped MgH_2.[9] Meanwhile, carbon-porous niobium pentoxide (C-p-Nb_2O_5) synthesized by a wet-chemical technique reduced the on-set dehydrogenation temperature about 181 °C due to the catalytic effect of Nb_2O_5, which was much lower than the pristine MgH_2.[10] Furthermore, adding ZrO_2 to MgH_2 improved the hydrogen storage performance due to the catalytic interaction of ZrO_2 with MgH_2 and formed active ZrH_x catalysts.[11] Transition-metal additives with Mg, appearing as either alloying or secondary particles, enhanced the hydrogen storage performance of MgH_2. In such cases, the addition of 4% Ni nanofibers (NFs) with MgH_2 using the ball milling method released

Received: January 6, 2024
Revised: February 19, 2024
Accepted: March 29, 2024
Published: April 22, 2024

© 2024 The Authors. Published by American Chemical Society

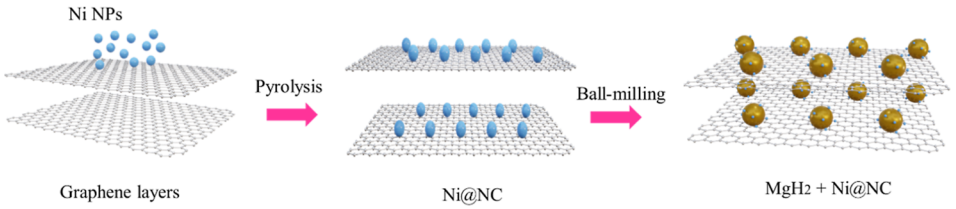

Figure 1. Schematic view of Ni NPs deposition on graphene layers, formation of Ni@NC nanostructure, and ball milling of MgH_2 and Ni@NC to form MgH_2 + Ni@NC nanocomposites.

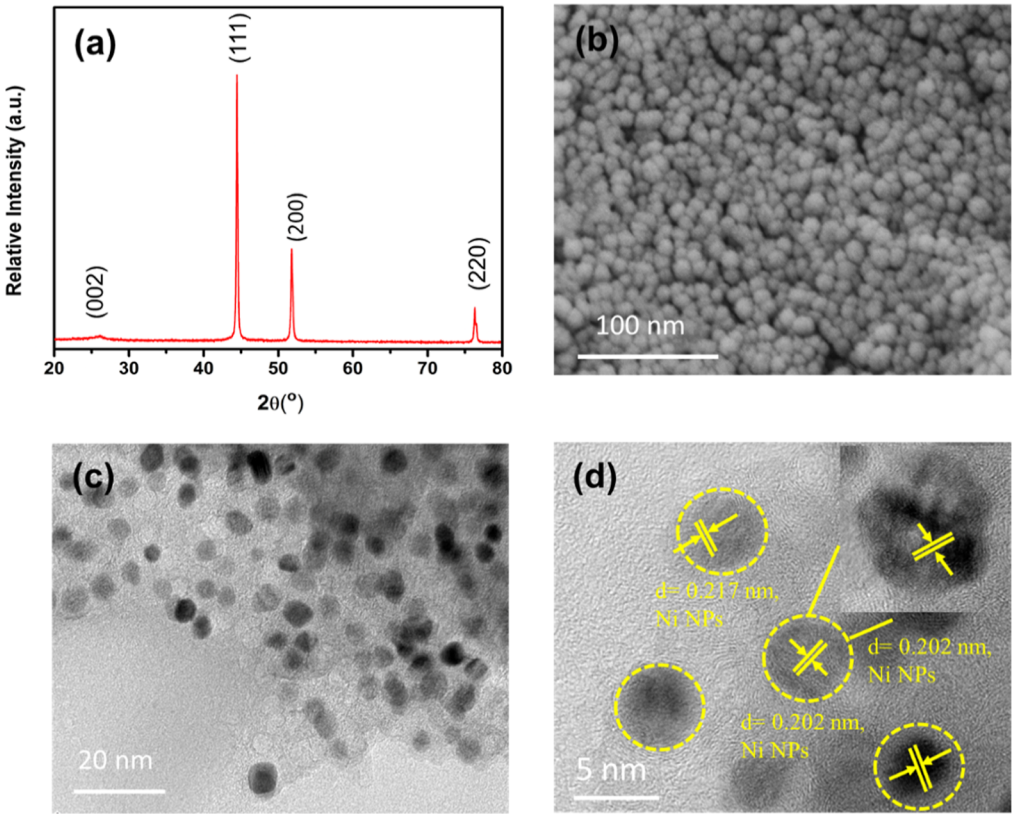

Figure 2. Structural and morphology results of the Ni@NC nanocomposite. (a) XRD patterns containing Ni and carbon peaks, (b) SEM morphology, (c) TEM microstructure, and (d) HRTEM observations of the Ni@NC nanocomposite.

hydrogen at an on-set temperature of 143 °C which dehydrogenated completely within 11 min at 325 °C (7.02 wt %).[12] The ultrathin Ni nanoparticles (NPs) (2−6 nm) were synthesized by the H_2 plasma reduction method using nickel acetylacetonate precursors and ball-milled with MgH_2. This composite rapidly released 6.5 wt % hydrogen in 10 min at 275 °C, while desorbed 6.0 wt % hydrogen at 225 °C. This remarkable improvement in the hydrogen-storage properties was attributed to the ultrafine and in situ formed $Mg_2NiH_{0.3}$ nanocrystals during the cycling process.[13] Xia et al.[14] studied that graphene-supported Ni NPs with MgH_2 boosted hydrogen storage properties, achieving a high reversible capacity of 5.5 wt % and long cyclic performance (100 cycles) owing to the thin size of MgH_2 and alloying with Ni NPs on the graphene surface. In another study, adding carbon NF-coated Ni NPs with Mg hydrides designed MgH_2-10 wt % Ni@C nanocomposites, which released hydrogen 5.91 wt % at 325 °C within 500 s due to catalytic behavior of highly dispersed Ni NPs.[15] Yao et al.[16] added 10 wt % Ni_4@rGO_6 with MgH_2 nanocomposites via ball-milling showed high hydrogen storage capacity (absorbed 5.0 wt % at 100 °C, while desorbed 6.1 wt % at 300 °C within 15 min), suggesting that the in situ formed Mg_2Ni/Mg_2NiH_4 during hydrogen ab/desorption cycles exhibited a better catalytic effect than Ni NPs. Another study showed that the addition of TiH_2 and graphite into Mg_2NiH_4 improved the surface oxidation performance coupled with the sorption kinetic rates. The Mg_2NiH_4−TiH_2 composition could readily desorb 2.36 wt % hydrogen within 400 s and absorb 2.33 wt % in 100 s at 230 °C. These results were attributed to the sacrificial effect of TiH_2 and in situ formed Ni-based composition.[17] Gao et al. studied flower-like Ni MOF with MgH_2 and reported that Ni effectively improved the hydrogen storage properties of MgH_2-5 wt % Ni MOF, absorbing 6.4 wt % H_2 at 300 °C within 600 s due to the coupling effect of in situ formed Mg_2Ni/Mg_2NiH_4, MgO NPs, amorphous C, and remaining layered Ni MOF.[18] Similarly, adding 5 wt % uniformly distributed Ni NPs on carbon to MgH_2 showed superior catalytic hydrogen storage performance and reduced the hydrogen on-set temperature to 187 °C.[19] Likewise, another class of two-dimensional (2D) materials called MXenes showed superior catalytic performance by adding Ni@Ti-MX to MgH_2 which reduced the dehydrogenation

https://doi.org/10.1021/acsomega.4c00198
ACS Omega 2024, 9, 19261−19271

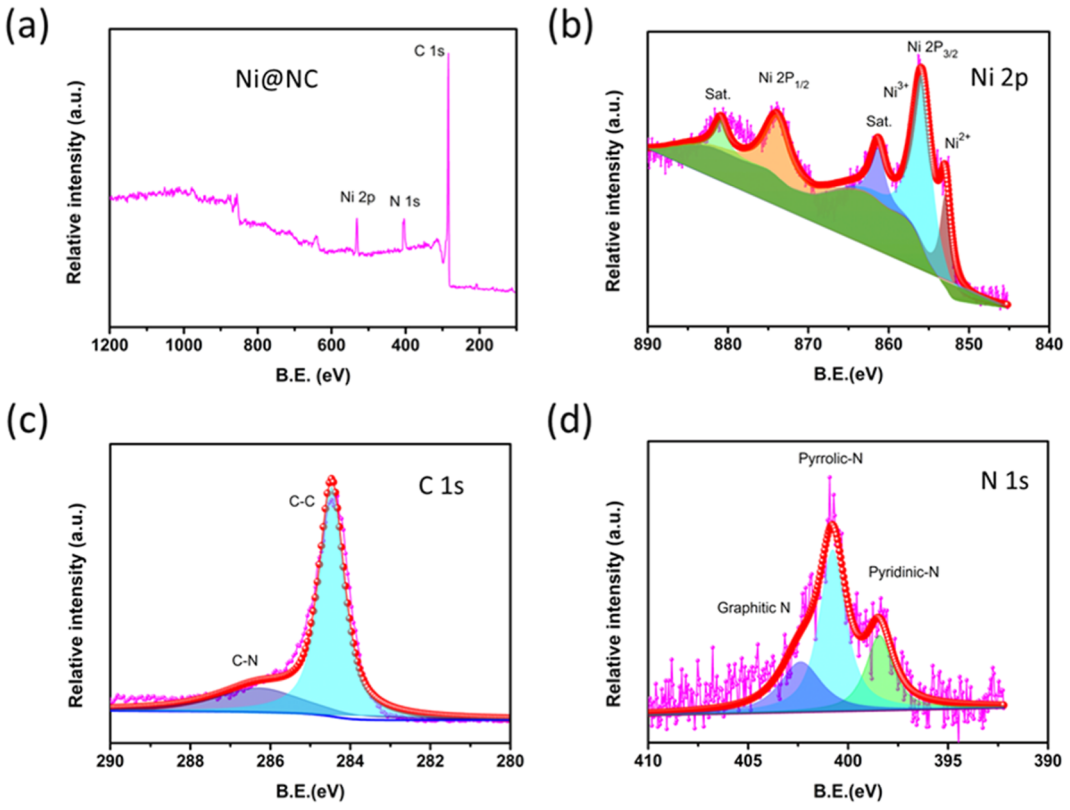

Figure 3. XPS results of the Ni@NC nanostructure. The survey curve (a), Ni 1s curve and fitted spectra (b), C 1s result with fitted curves (c), and (d) N 1s with fitted curves.

temperature by 221 °C while absorbed 5.4 wt % hydrogen within 25 s at 125 °C and desorbed 5.2 wt % in 15 min at 250 °C due to multiphasic effects of Mg and catalysts.[20,21] In addition, adding a few-layer MXene $Ti_3C_2T_x$-supported Ni@C nanoflakes to MgH_2 showed a remarkable cyclic performance of 50 cycles with negligible capacity loss due to the formation of Mg_2NiH_4 and highly dispersed metallic Ti NPs.[22] Porous carbon and nitrogen-doped graphene material have also been studied to adsorb/absorb hydrogen and improve the kinetic performance due to unique electronic properties.[23] Nitrogen doping has been investigated to enhance the hydrogen storage performance of MgH_2. In this study, heteroatom doping was studied in terms of bonding configurations and heteroatom doping concentrations. The graphene−Mg nanocomposites doped with heteroatoms; hydrogen uptake was enhanced with significantly low activation energy during the early stages of desorption, perhaps due to the facilitation of nucleation.[24] Another study showed that N-doped graphene nanoribbons enhanced the hydrogen sorption kinetics of Mg hydrides due to the nitrogen doping and encapsulation effect.[25] Theoretically, studies showed that the N-doped graphene layers reduced the adsorption energy due to electronic behavior and higher electronegativity than carbon.[26] Although, tremendous efforts have been devoted to improving the hydrogen storage performance of MgH_2; these investigations are still suffering from fast sorption kinetic rates, long cycle life, and low dehydrogenation temperature. This may be due to the agglomeration of MgH_2 NPs during preparation or using low-efficiency catalysts to dissociate Mg−H bonds at low temperatures.

In this paper, we have focused on the designing and preparation of nitrogen-doped carbon-supported Ni NPs and ball-milled with MgH_2, aiming to improve hydrogen storage, and reduce the dehydrogenation temperature and cyclic performance. The obtained structure MgH_2 + 15 wt % Ni@NC is capable of reducing the dehydrogenation temperature to 195 °C, fast sorption kinetic performance, and long cycle life. This composite uptakes 5.5 wt % hydrogen at 100 °C while achieving 6.5 wt % capacity at 275 °C, which are better than other compositions and pristine MgH_2. In addition, the composite achieved 1.7 and 6.5 wt % desorption capacities at 225 and 300 °C temperature, respectively. The MgH_2 + 15 wt % Ni@NC nanocomposite shows high cyclic stability, achieving 98.0% capacity retention after 100 sorption kinetic cycles at 270 °C.

RESULTS AND DISCUSSION

Structural and Morphological Characteristics of Ni@NC Nanostructure. The Ni@NC nanostructures were formed by the addition of Ni NPs on the surface graphene layers, which act as a strong support for NP growth. The thermolysis process results in the wrapping of Ni NPs in graphene layers with nitrogen-doping content.[27,28] The abundance of functional groups and C−C cleavage result in the development of Ni@NC nanostructure with uniform size and morphology. Furthermore, the Ni@NC nanostructures were treated with MgH_2 to form MgH_2 + Ni@NC nanocomposites via ball milling as shown in Figure 1.

The phase analysis and morphology micrographs of the Ni@NC nanostructures are shown in Figure 2. The X-ray diffraction (XRD) pattern shows that the major peaks are corresponded to Ni NPs, exhibiting cubic structure with space group $[Fm\bar{3}m(225)]$, whereas a small peak of carbon is indexed at 2θ = 26.5°. After annealing at 900 °C for 1 hr, the

https://doi.org/10.1021/acsomega.4c00198
ACS Omega 2024, 9, 19261−19271

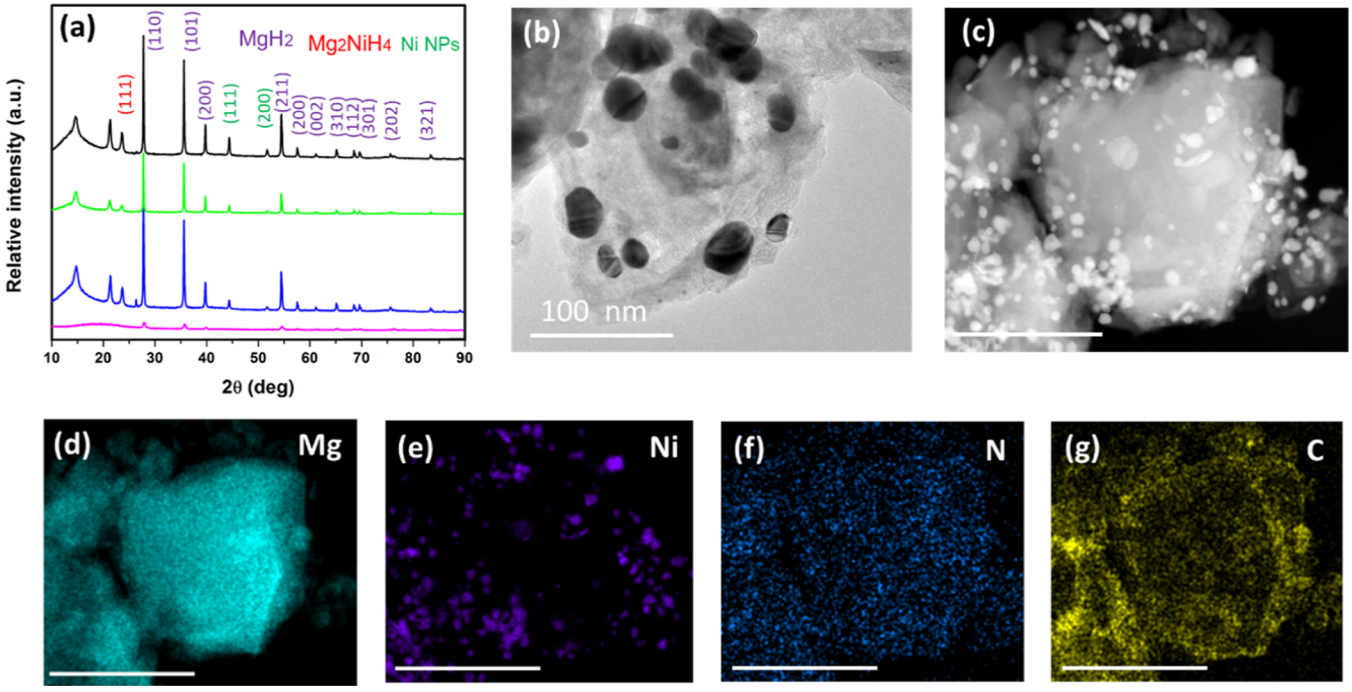

Figure 4. (a) XRD results of MgH_2 + 15 wt % Ni@NC (black), MgH_2 + 10 wt % Ni@NC (green), MgH_2 + 5 wt % Ni@NC (blue), and MgH_2 (pink) and (b) TEM morphology results and (c−g) scanning transmission electron microscopy-high-angle annular dark-field (STEM-HAADF) results of MgH_2 + 15 wt % Ni@NC.

graphene layers are wrapped over the Ni NPs, and the Ni@NC composite is formed. The scanning electron microscopy (SEM) results of Figure 2b indicate that ultrasmall size graphene-wrapped Ni NPs are uniformly dispersed.. The size of Ni NPs is calculated about 10 nm, which are uniform in size and shape. These results also indicate that graphene wrapping prevents the size growth of Ni NPs and avoids agglomeration. Transmission electron microscopy (TEM) results also indicate that Ni NPs are covered by a few layers of graphene with a uniform distribution, as shown in Figure S1. The robustly bonded metal−matrix interface facilitates the sustained dispersion of the catalyst, leading to an enlarged availability of exposed active sites and consequently enhancing the catalytic activity.[29] The size of Ni NPs calculated by TEM is about 5−8 nm, which is smaller than the SEM observations. High-resolution TEM (HRTEM) observations reflect that the *d*-spacings d = 0.202 and d = 0.217 nm correspond to Ni NPs with different planes which can be indexed as (111) and (220), respectively. These structural results match well with XRD results.

To further investigate the elemental analysis and chemical states of the Ni@NC NPs, the X-ray photoelectron spectroscopy (XPS) test was performed, and the results are presented in Figure 3. According to these results, the major peaks of survey curves correspond to Ni 2p, C 1s, and N 1s states of Ni@NC. The Ni 2p curve is fitted to two main peaks Ni $2p_{1/2}$ and Ni $2p_{3/2}$, which are positioned at 873.9 and 855.9 eV, respectively. The Ni $2p_{3/2}$ spectrum further divides into Ni^{2+}, Ni^{3+}, and satellite curves at different energy positions 853.1, 855.0, and 861.2 eV, respectively, which can be observed in the previous study.[30] The C 1s curve further splits into C−C and C−N spectra located at 284.6 and 286.5 eV, respectively. Similarly, the N 1s curve also splits into graphitic-N, pyrrolic-N, and pyridinic-N spectra located at 402.5, 400.8, and 398.5 eV, respectively. The XPS results confirm N-doping, indicating that the graphene structure is modified due to N-doping. These results show the formation of Ni@NC NPs.

Structural and Morphology Results of MgH_2 + *x* wt % Ni@NC Nanocomposites. The MgH_2 + *x* wt % Ni@NC nanocomposites were synthesized via ball milling adding Ni@NC nanocomposites to Mg hydride powder in the hydrogen environment for 5 hrs. Three distinct composites were synthesized, exhibiting different weight ratios of Ni@NC NPs (wt % of 5, 10, and 15) in combination with MgH_2.

From the XRD patterns of Figure 4, the major peaks are indexed to MgH_2 with the tetragonal structure of the space group $P4_2/mnm(136)$. The other phases, such as Mg_2NiH_4 and Ni NPs, are observed as secondary phases. During the ball milling process, the Ni NPs are alloyed with MgH_2 which lead to the formation of Mg_2NiH_4.[16,31,32] The TEM results indicate that the Ni NPs reacted with MgH_2 during the ball milling process, growing the MgH_2 + 15 wt % Ni@NC nanocomposite on the graphene layers. The STEM−EDS observations reflect that the Ni NPs and MgH_2 NPs are evenly distributed in the microstructure. In addition, the mapping results of the MgH_2 + 15 wt % Ni@NC nanocomposite indicate that Ni NPs are distributed on MgH_2 nanostructures. These nanostructures comprise varied nanocrystalline structures including Ni NPs, MgH_2, and Mg_2NiH_4 nanocomposites. These results indicate that mostly Ni NPs are reacted with MgH_2 to synthesize the Mg_2NiH_4 nanocomposite during ball milling. The secondary small-sized NPs Ni NPs on the surface of graphene layers and are also overserved. In addition, these observations reveal that Ni@NC prevents agglomeration of the MgH_2 nanostructure. These results match well with XRD patterns. Furthermore, SEM/EDS mapping shows that Ni NPs, N, C, and MgH_2 are distributed in the microstructure abundantly, as shown in Figure 5. EDS results show that the major part of the composite is MgH_2, while the doping materials such as Ni and N contribute to the elemental composition. Oxygen content in

https://doi.org/10.1021/acsomega.4c00198
ACS Omega 2024, 9, 19261−19271

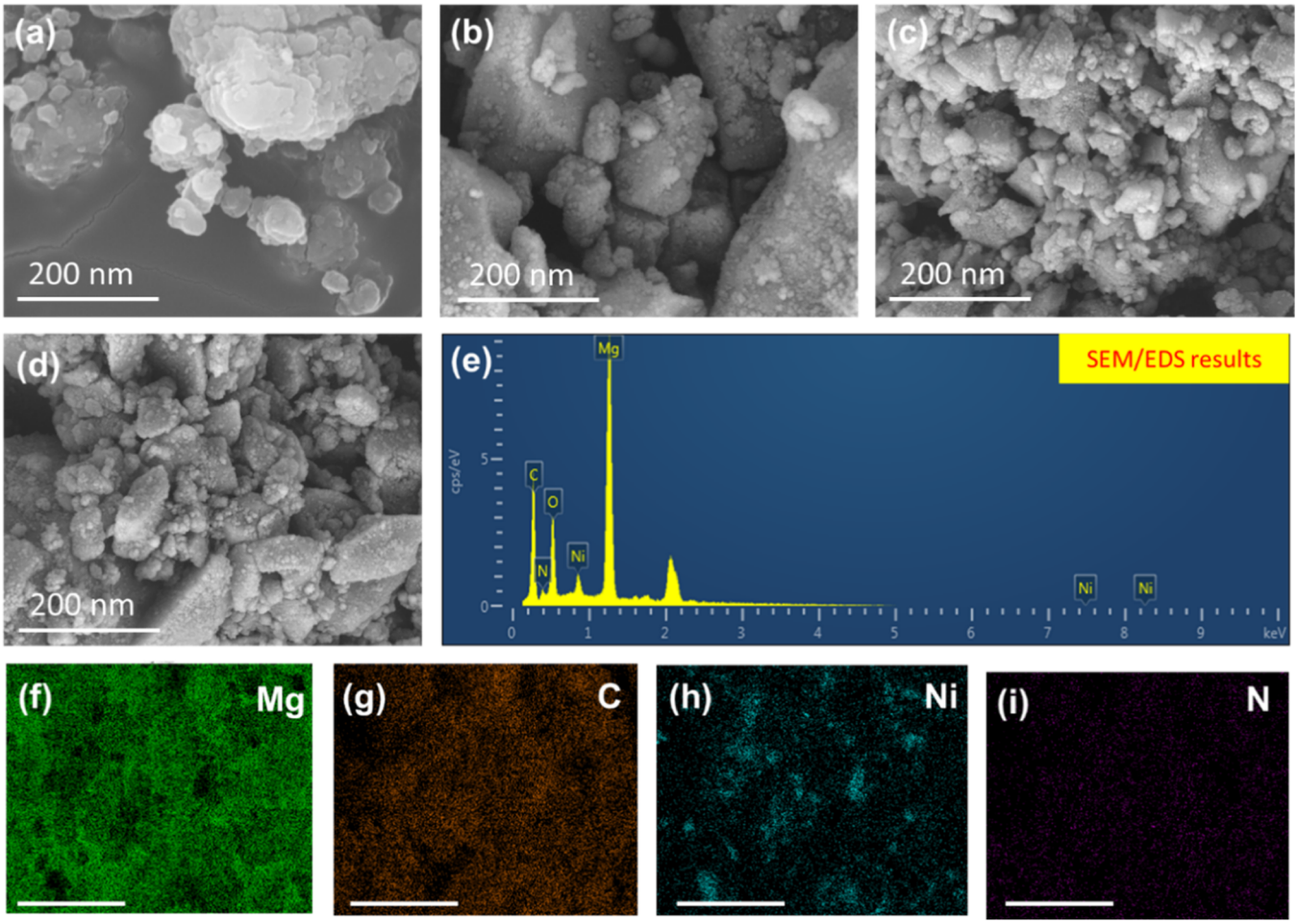

Figure 5. (a–d) SEM morphology results of MgH_2, MgH_2 + 5 wt % Ni@NC, MgH_2 + 10 wt % Ni@NC, and MgH_2 + 15 wt % Ni@NC and (e) SEM/energy-dispersive spectroscopy (EDS) results and (f–i) SEM/EDS mapping of the MgH_2 + 15 wt % Ni@NC nanocomposite.

the microstructure is observed due to the sample transferring from the glovebox to the SEM sample chamber.

To in-depth investigate the elemental states of the doping contents and MgH_2 after the ball-milling process, the XPS test of the MgH_2 + 15 wt % Ni@NC hydrogenated sample was performed and the results are mentioned in Figure 6. From the XPS spectra, the Mg 1s peak is located at 1303.03 eV along with a small spectrum of Mg $(OH)_2$/MgO at 1304.20 eV which comes from the surface oxidation during sample transformation for the XPS test. In addition, C 1s spectra are fitted to C−C (284.60 eV), C−N (287.05 eV), and C═O (292.81 eV) spectra, indicating that N is doped in the carbon matrix with oxygen functionality on the surface. Similarly, the Ni 2P spectrum is fitted to two main curves Ni $2P_{1/2}$ and Ni $2P_{3/2}$, while Ni $2P_{1/2}$ further divides into Ni metal and satellite curves, which are positioned at 273.40 and 277.50 eV, respectively. In addition, the Ni $2P_{3/2}$ curve is further fitted to Ni, satellite, and a minor peak of Ni^{3+} located at 250.20, 860.50, and 862.25 eV, respectively. This indicates that the Ni ions transferred to metallic states during the ball-milling process and alloying with Mg.[28] Similarly, the N 1s curve also splits into graphitic-N, pyrrolic-N, and pyridinic-N spectra, which are located at 401.50, 400.10, and 399.05 eV, respectively. These results indicate that the Ni@NC NPs are added to the MgH_2 matrix after balling which remarkably contributes to the hydrogenation/dehydrogenation process.

Hydrogen Storage Performance Measurements. The hydrogen storage measurements of the MgH_2 + x wt % Ni@NC (where x = 0, 5, 10, 15) nanocomposites were carried out using a PCT machine. Initially, the temperature-programmed desorption (TPD) test measures the hydrogen desorption performance at increasing temperature under a constant rate, 5 °C/min, as shown in Figures 7 and S2. The MgH_2 + 15 wt % Ni@NC nanocomposite decomposes first and releases hydrogen at an on-set temperature of 195 °C, which is faster compared to other composites, as shown in Figure 7a. The hydrogen release content from the TPD test is higher than the theoretical capacity of MgH_2 + 15 wt % Ni@NC. This contribution may come from the impurities or loosely attached hydrogen on the sample surface, releasing hydrogen during the TPD test. Two distinct plateaus can be observed during the hydrogen release, indicating that the composite consists of Mg_2NiH_4 and MgH_2, which release hydrogen at varied temperatures. These in situ Mg_2NiH_4 nanostructures provide more channels for hydrogen absorption and release. This varied phase and microstructure can also be observed in XRD and microstructure analysis. Figure 7b summarizes the hydrogen absorption capacities of various composites at different temperatures and 30 bar pressure, indicating that MgH_2 + 15 wt % Ni@NC shows superior hydrogen storage performance compared to other composites. The stability of the MgH_2 + 15 wt % Ni@NC nanocomposite is determined by the sorption cyclic performance at 270 °C under vacuum of 30

https://doi.org/10.1021/acsomega.4c00198
ACS Omega 2024, 9, 19261−19271

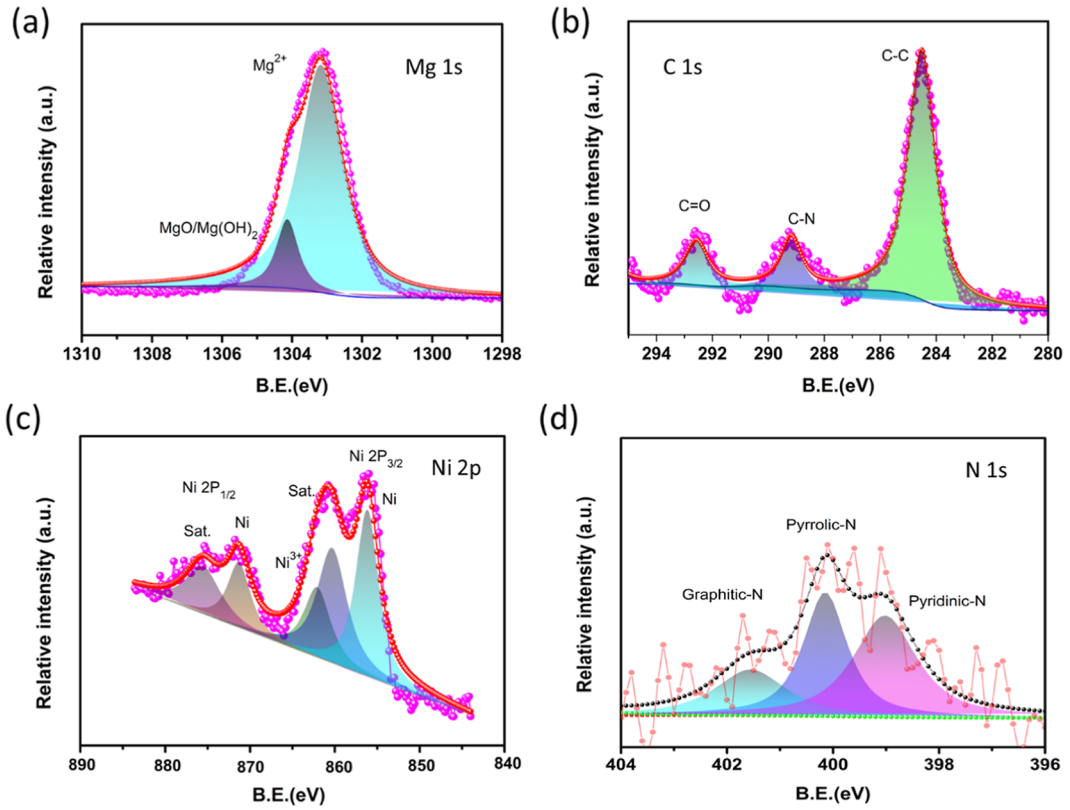

Figure 6. XPS results of the MgH_2 + 15 wt % Ni@NC hydrogenated nanocomposite after ball milling: (a) Mg 1s, (b) C 1s, (c) Ni 2p, and (d) N 1s.

and 0.01 bar for absorption and desorption, respectively; the results are shown in Figure 7c,d). The results elucidate that MgH_2 + 15 wt % Ni@NC absorbs and desorbs hydrogen rapidly, achieving a high capacity of around 6.0 wt %. After 100 cycles of sorption kinetics, MgH_2 + 15 wt % Ni@NC attributes the negligible loss in reversible capacity, which manifests that this composite is highly stable even after cycle performance. This remarkable stability is due to the presence of the Ni@NC nanostructure, which prevents the microstructure from deformation during cyclic performance under high temperature and pressure. In addition, the Ni@NC-supported Mg hydride structure is capable of precluding the agglomeration of MgH_2 NPs after successive sorption cycles. Thus, the Ni@NC nanocatalyst reduces the dehydrogenation temperature as well as improves the sorption kinetic rates and cyclic stability of MgH_2.

To further investigate the effect of Ni NPs on hydrogen storage performance, the isothermal sorption kinetic rates were measured at various temperatures with 30 and 0.01 bar hydrogen pressure, respectively. Figure 8 indicates that the MgH_2 + 15 wt % Ni@NC nanocomposite absorbs hydrogen much more rapidly compared to other composites. Interestingly, MgH_2 + 15 wt % Ni@NC composition uptakes 5.2 wt % hydrogen in 1 hr at 30 bar, while MgH_2 + 10 wt % Ni@NC and MgH_2 + 5 wt % Ni@NC achieve 4.1 and 3.5 wt % hydrogen capacities at 100 °C, respectively. Likewise, MgH_2 + 15 wt % Ni@NC achieves the highest absorption capacity of 6.5 wt % at 275 °C and 30 bar. The desorption kinetic rates were measured at 0.01 bar and varied temperatures, as shown in Figure 9. To investigate the role of the catalyst in the hydrogen storage capacity, absorption kinetic tests of sample Ni@NC were performed at various temperatures, and the results are mentioned in Figure S3. These results indicate that hydrogen storage capacity is negligible compared to MgH_2, showing that Ni@NC may not contribute to hydrogen storage capacity and exhibits the catalytic role during the hydrogenation process. In addition, for comparison, the kinetic rates of the MgH_2 + 15 wt % Ni@rGO sample were tested at different temperatures (Figure S4), indicating that the MgH_2 + 15 wt % Ni@NC nanocomposite takes up hydrogen more rapidly than the Ni@rGO-doped sample.

The results show that the MgH_2 + 15 wt % Ni@NC nanocomposite releases hydrogen 1.7 wt % at 225 °C, which is higher than other compositions and pristine MgH_2. Moreover, the highest desorption capacity about 6.3 wt % is achieved within 15 min by the MgH_2 + 15 wt % Ni@NC nanocomposite. Compared to other compositions, this capacity is substantially higher and more rapid at the same temperature. The remarkably improved performance of MgH_2 + 15 wt % Ni@NC is due to the catalytic behavior of nanosized Ni NPs on N-doped graphene thin layers. In addition, the nitrogen-doping effect coupled with Ni NPs may highly contribute to the improvement of hydrogen storage performance.

Catalytic Role of Ni@NC Nanostructure and Reaction Mechanism. The catalytic performance of the Ni@NC nanostructure on the hydrogen storage performance of MgH_2 is investigated. To in-depth investigate the structure and morphology after hydrogenation/dehydrogenation cyclic performance, the XRD and HRTEM analysis tests were performed. After full dehydrogenation of the MgH_2 + 15 wt % Ni@NC nanocomposite, the phase evolution results are shown in Figure 10. In the microstructures, the Mg_2Ni phase exhibited a hexagonal structure [PDF#35-1225 with a space

https://doi.org/10.1021/acsomega.4c00198
ACS Omega 2024, 9, 19261−19271

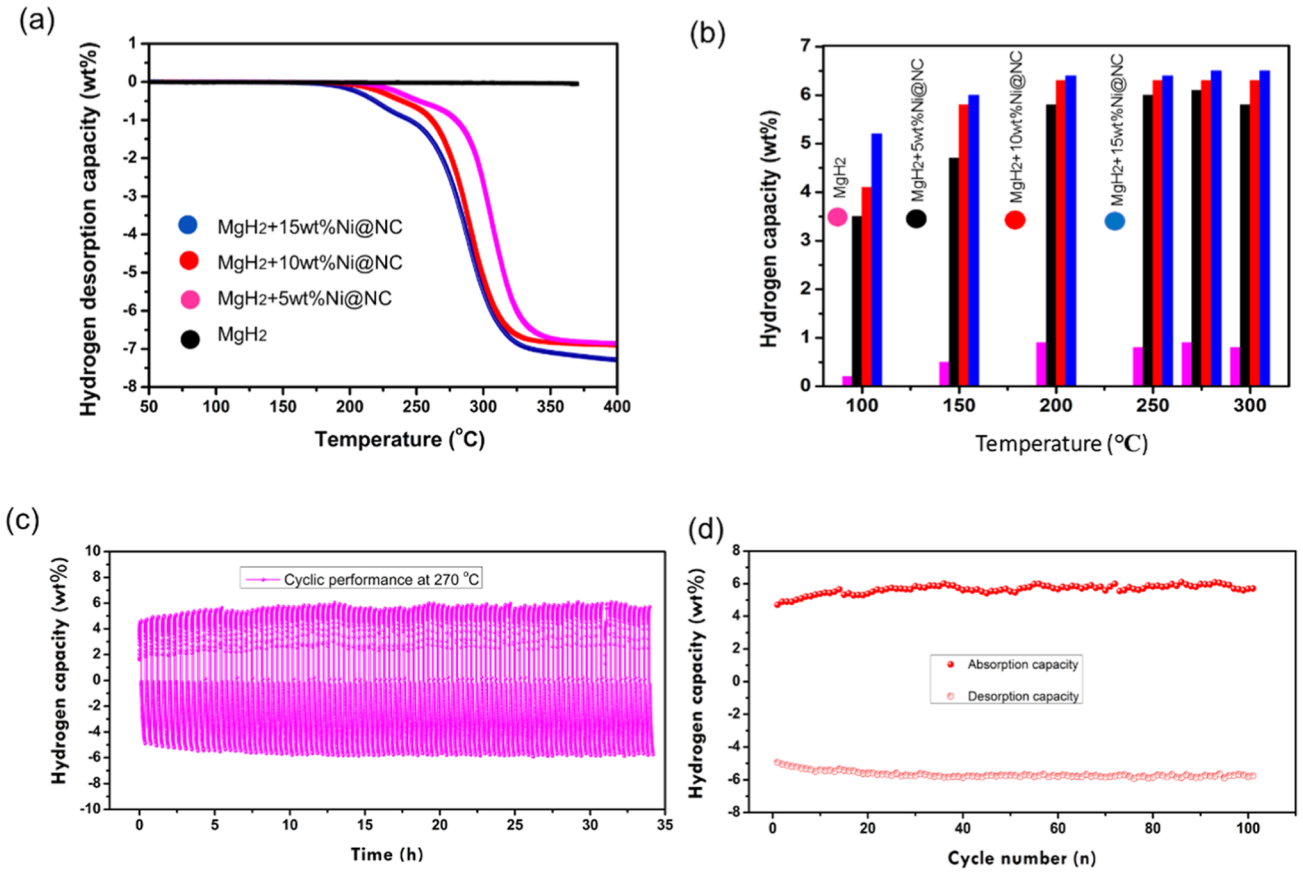

Figure 7. (a) TPD performance of MgH_2, MgH_2 + 5 wt % Ni@NC, MgH_2 + 10 wt % Ni@NC, and MgH_2 + 15 wt % Ni@NC nanocomposites with increasing temperature. (b) Hydrogen absorption capacities of different compositions at various temperatures. (c,d) Cyclic performance of the MgH_2 + 15 wt % Ni@NC nanocomposite at 270 °C.

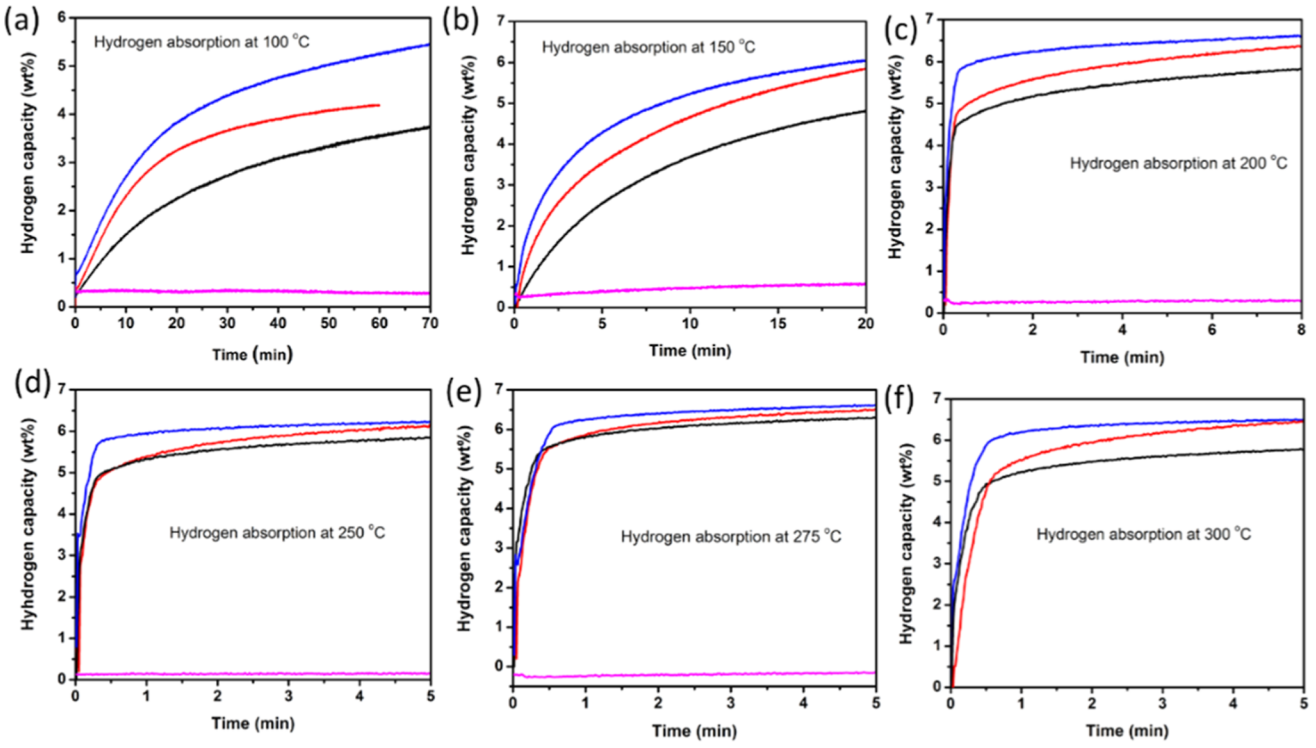

Figure 8. (a–f) Absorption kinetic performance of MgH_2 (pink), MgH_2 + 5 wt % Ni@NC (black), MgH_2 + 10 wt % Ni@NC (red), and MgH_2 + 15 wt % Ni@NC (blue) at 30 bar and varied temperature.

https://doi.org/10.1021/acsomega.4c00198
ACS Omega 2024, 9, 19261−19271

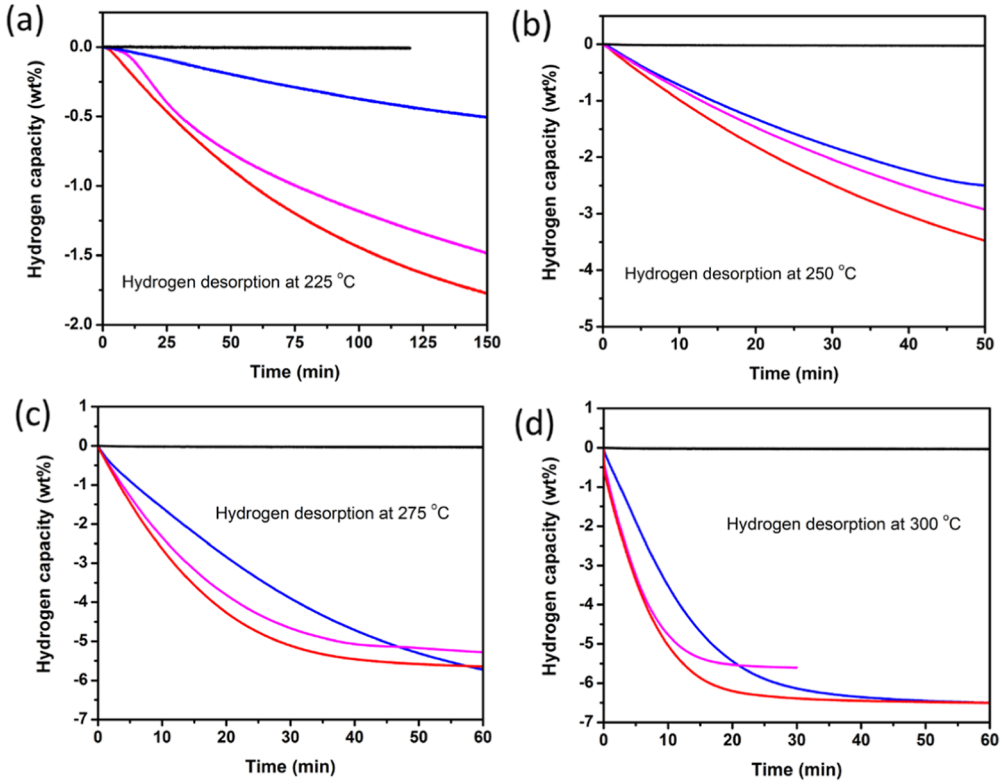

Figure 9. (a–d) Desorption kinetic performance of MgH_2 (black), MgH_2 + 5 wt % Ni@NC (blue), MgH_2 + 10 wt % Ni@NC (pink), and MgH_2 + 15 wt % Ni@NC (red) at 0.01 bar and varied temperature.

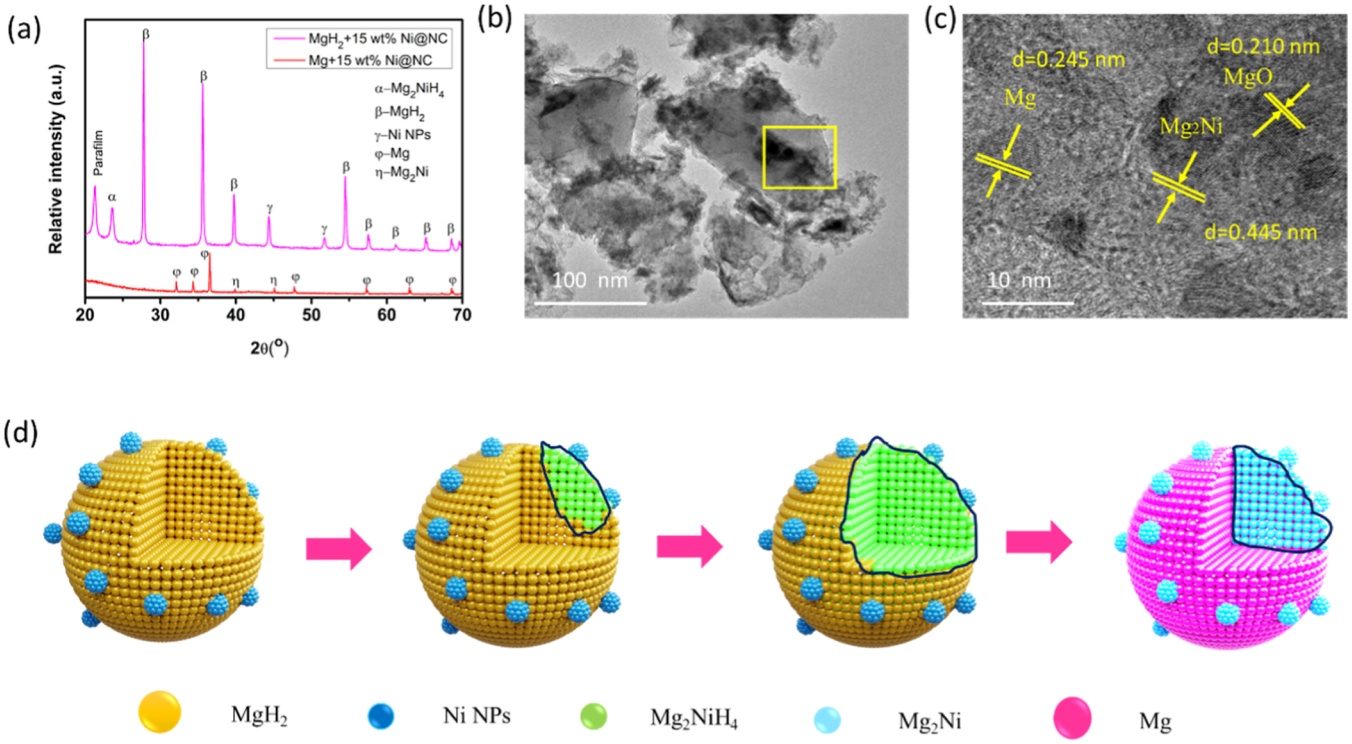

Figure 10. (a) XRD results of the MgH_2 + 15 wt % Ni@NC nanocomposite before and after the hydrogenation. (b,c) HRTEM results of the MgH_2 + 15 wt % Ni@NC nanocomposite after the cyclic performance. (d) Schematic of MgH_2 and Mg_2NiH_4 formation and transformation after the hydrogen release.

group of $P6_222$ (180)] along with the Mg phase unveiling a hexagonal structure (PDF#35-0821) and space group [$P6_3/mmc$ (194)] are noticed. The Ni NPs are not detected after dehydrogenation of the sample in the XRD results. Besides, MgO can also be detected which may be due to the surface oxidation during sample transferring to the TEM chamber.

https://doi.org/10.1021/acsomega.4c00198
ACS Omega 2024, 9, 19261−19271

This may further indicate that the sample is fully dehydrogenated, and the MgH_2 and Mg_2NiH_4 phases are transferred to Mg and Mg_2Ni.

Hydrogeneration reaction

$$3Mg + Ni + 3H_2 \rightarrow MgH_2 + Mg_2NiH_4 \quad (1)$$

Dehydrogenation reaction

$$MgH_2 \rightarrow Mg + H_2\uparrow \quad (2)$$

$$Mg_2NiH_4 \rightarrow Mg_2Ni + H_2\uparrow \quad (3)$$

In addition, HRTEM results are presented in Figure 10b,c, indicating that after the hydrogen release, the MgH_2 phase is transferred to Mg(101) with a *d*-spacing of 0.245 nm. Furthermore, the Mg_2NiH_4 phase is converted to Mg_2Ni(003) with a *d* spacing of 0.445 nm. These results are well-consistent with XRD results and can be found in previous reports.[29] Besides, Ni NPs are not detectable in the HRTEM micrographs, suggesting that the Ni NPs were completely alloying with Mg and generated Mg_2Ni in the dehydrogenation of the MgH_2 + 15 wt % Ni@NC nanocomposite, which agrees with the result of XRD.[33,34] Similarly, the hydrogenation and dehydrogenation reactions of Mg and Ni NPs also indicate the phase transformation, as shown in eqs 1−3, implying that Mg_2Ni and Mg yield after releasing hydrogen. In consideration of our experimental observations, we present a schematic diagram encapsulating the hydrogen absorption and desorption phenomena of the MgH_2 + 15 wt % Ni@NC nanocomposite, alongside an exposition of the catalytic mechanisms inherent to Ni@NC, as shown in Figure 10d. In the first step, Mg is milled with Ni NPs in a H_2 environment to form MgH_2 and Mg_2NiH_4, while Ni NPs are distributed on the MgH_2 surface. However, a minor part of MgH_2 is composed of Mg_2NiH_4, growing further in the next step, which is also indicated from the HRTEM and XRD results of Figure 4. In the dehydrogenation step, hydrogen is released and Mg_2Ni and Mg NPs are noticed, which can also be observed in HRTEM and XRD results of Figure 10.

The substantial improvement in hydrogen storage performance of MgH_2 + 15 wt % Ni@NC is due to the catalytic performance of the Ni@NC composite and in situ formed in situ Mg_2NiH_4 compared to additive-free MgH_2. During the ball-milling process, the Ni NPs and in situ Mg_2NiH_4 nanocomposite are formed which play a vital role in decomposition of Mg−H bonds at low temperatures, and consequently, the on-set temperature is reduced to 195 °C, which is much lower than pristine Mg hydride.[16,31,34] On one side, these nanostructures promote the hydrogenation/dehydrogenation process, reducing the bond length and in the other side stabilize the MgH_2 nanocrystallines. The uniform distribution of Ni NPs in microstructure could promote the hydrogen sorption performance and releases hydrogen rapidly.[19,35] In addition, graphene-supported Ni NPs provide multiple channels to promote the dehydrogenation and sorption performances of MgH_2.[36] Previously, it was proposed that the spontaneous generation of Mg_2NiH_4 on the rGO surface can function as a "hydrogen pump," thereby improving the kinetics of dehydrogenation.[29,33] The absorption and desorption kinetic rates could be promoted due to the Ni NPs and the in situ-formed Mg_2NiH_4 nanocomposite, indicating that these nanocatalysts exhibit a dual strategy of enhancing the hydrogen storage performance of MgH_2. Furthermore, Ni promotes the nucleation of magnesium phases and facilitates the recombination of hydrogen atoms, resulting in faster desorption kinetic rates.[32,34] In addition, N-doping can also improve the catalytic properties of the MgH_2 surface, which can promote the dissociation of hydrogen molecules and improve the hydrogen uptake kinetics. The nitrogen-induced graphene structure modifies the electronic arrangement within the structure which can let down the activation energy barrier for hydrogenation, making the hydrogen uptake process faster.[24,25] Similarly, compared to undoped graphene, the N-doping graphene structure facilitates the hydrogen absorption/release process due to high electronegativity, pulling hydrogen from the Mg surface.[37,38] The multiphasic regions in the HRTEM microstructures provide numerous channels for hydrogen absorption and desorption and facilitate the kinetic rates significantly. With the increasing catalyst-loading mass, the hydrogenation performance further improves, indicating that the high loading mass is beneficial to the sorption and dehydrogenation performance of MgH_2.

CONCLUSIONS

In this study, we have designed nitrogen-doped graphene-supported Ni NPs, aiming to investigate the catalytic effects on reducing the dehydrogenation temperature and faster sorption kinetic rates of MgH_2. The results indicated that the dehydrogenation temperature was reduced to 195 °C of the MgH_2 + 15 wt % Ni@NC composite, which was 155 °C lower than that of pristine MgH_2. The MgH_2 + 15 wt % Ni@NC composition absorbed 5.5 wt % at 100 °C while achieving a capacity 6.5 wt % at 275 °C hydrogen. This composition achieved 1.7 and 6.5 wt % desorption capacities at 225 and 300 °C temperature, respectively, which was faster than other compositions and pristine MgH_2. In addition, this composite reached 100 sorption kinetic cycles with 98.0% capacity retention at 270 °C due to the highly stable structure. The in situ formed Mg_2NiH_4 NPs and multiphasic structure provided abundant channels for the hydrogen absorption/desorption process. This approach unveils an opportunity to synthesize high-performance MgH_2 for large-scale applications.

MATERIAL SYNTHESIS

Preparation of Ni@NC Nanostructures. The synthesis of the Ni@NC nanostructure was carried out by using the thermolysis method. To start with, $Ni(NO_3)_2{\cdot}6H_2O$ (0.5 mmol) was dissolved in 30 mL of dimethylformamide (DMF) by stirring to produce graphene-wrapped Ni NPs. Subsequently, ethylenediaminetetraacetic acid (0.5 mmol) containing 5 mg/mL graphene oxide was dissolved in 20 mL of DMF using ultrasonication, followed by the dropwise addition of *N*,*N*,*N*-triethylamine (0.02 mmol) (6 mL). The mixture of the two solutions resulted in the formation of a greenish-colored precipitate. The precipitate was washed with DMF, centrifuged, and vacuum-dried at 60 °C overnight. The gray-colored powder was obtained after annealing for an hr at 5 °C per minute at 900 °C under an argon atmosphere.

Synthesis of MgH_2 + *x* wt % Ni@NC Nanocomposites. The MgH_2 + *x* wt % Ni@NC nanocomposites were synthesized by adding 5, 10, and 15 wt % of Ni@NC nanostructure to MgH_2 powder in a stainless-steel jar with a ball-to-powder ratio of 40:1. The mixture was ball-milled for 5 h in a hydrogen environment. For comparison, the MgH_2 + 15 wt % Ni@rGO and pure MgH_2 samples were ball-milled under the same conditions. To avoid surface oxidation reactions, the

https://doi.org/10.1021/acsomega.4c00198
ACS Omega 2024, 9, 19261−19271

samples were prepared and handled in a glovebox with O_2 and H_2O levels ≤0.01 ppm.

Material Characterization. The synthesized Ni@NC NPs and MgH_2 + x wt % Ni@NC (where x = 0, 5, 10, 15) nanocomposites were analyzed by XRD to confirm the phases and structural characteristics. The morphology micrographs of the synthesized nanocomposites were studied by using SEM coupled with SEM-EDS (Gemini SEM 500). To investigate the structure, phases, and elemental distribution within the composite, HRTEM (Thermo-Fisher Talos-F200X) and HAADF-STEM techniques were employed. To find out the elemental states, the XPS spectra were achieved using a Thermo Fisher ESCALAB Xi + instrument using monochromatic Al K sources. The hydrogen storage performances of the MgH_2 + x wt % Ni@NC (where x = 0, 5, 10, 15) nanocomposites were evaluated using a Sievert's-type pressure, composition, and temperature (P−C-T) apparatus. For each composition, a 100 g sample weight was used to measure the hydrogen storage performance. The hydrogen release performance was analyzed using a TPD technique with a rate of 5 °C/min. The sorption kinetic rate and cyclic performance were measured at various temperatures and pressures.

■ ASSOCIATED CONTENT

Supporting Information

The Supporting Information is available free of charge at https://pubs.acs.org/doi/10.1021/acsomega.4c00198.

TEM results of Ni@NC and TPD and kinetic performance of MgH_2 + 15 wt % and Ni@NC MgH_2 + 15 wt % Ni@rGO nanocomposites (PDF)

■ AUTHOR INFORMATION

Corresponding Authors

Wajid Ali − *Key Laboratory of Advanced Catalytic Materials (Ministry of Education), School of Materials Science and Chemistry, Zhejiang Normal University, Zhejiang Jinhua 321004, P. R. China;* orcid.org/0000-0001-8021-4313; Email: wajid_ali@zjnu.edu.cn

Rong Zhang − *School of Materials Science and Engineering, Changzhou University, Changzhou 213164, P. R. China*; Email: rzhang@cczu.edu.cn

Authors

Imran Muhammad − *School of Materials Science and Engineering, Changzhou University, Changzhou 213164, P. R. China*

Jaffer Saddique − *Key Laboratory of Advanced Catalytic Materials (Ministry of Education), School of Materials Science and Chemistry, Zhejiang Normal University, Zhejiang Jinhua 321004, P. R. China*

Chengzhang Wu − *State Key Laboratory of Advanced Special Steel, Key Laboratory of Advanced Ferrometallurgy, School of Materials Science and Engineering, Shanghai University, Shanghai 200072, China*

Muneeb ur Rahman − *Department of Physics, Islamia College Peshawar, Khyber Pakhtunkhwa 25120, Pakistan*

Zaheen Ullah Khan − *Institute of Materials for Energy and Environment, School of Materials Science and Engineering, Qingdao University, Qingdao 266071, China*

Complete contact information is available at: https://pubs.acs.org/10.1021/acsomega.4c00198

Notes

The authors declare no competing financial interest.

■ ACKNOWLEDGMENTS

We highly acknowledge the support from the Jiangsu Innovative & Entrepreneurial Talent group program (2017.37), "Six talent peaks" team project in Jiangsu Province (SWYY-CXTD-001), International Cooperation Project of Changzhou City (CZ20190019), and the Priority Academic Program Development (PAPD) of Jiangsu Higher Education Institutions. This work is also supported by the initial scientific research grant of Zhejiang Normal University (YS304322928).

■ REFERENCES

(1) Schlapbach, L.; Züttel, A. Hydrogen-storage materials for mobile applications. *Nature* **2001**, *414*, 353−358.

(2) Ouyang, L.; Chen, W.; Liu, J.; Felderhoff, M.; Wang, H.; Zhu, M. Enhancing the Regeneration Process of Consumed NaBH4 for Hydrogen Storage. *Adv. Energy Mater.* **2017**, *7*, 1700299.

(3) Liu, C.; Li, F.; Ma, L. P.; Cheng, H. M. Advanced materials for energy storage. *Adv. Mater.* **2010**, *22*, E28−E62.

(4) Mohtadi, R.; Orimo, S.-I. The renaissance of hydrides as energy materials. *Nat. Rev. Mater.* **2016**, *2*, 16091.

(5) Au, Y. S.; Obbink, M. K.; Srinivasan, S.; Magusin, P. C. M. M.; de Jong, K. P.; de Jongh, P. E. The Size Dependence of Hydrogen Mobility and Sorption Kinetics for Carbon-Supported MgH2 Particles. *Adv. Funct. Mater.* **2014**, *24*, 3604−3611.

(6) Xia, G.; Tan, Y.; Chen, X.; Sun, D.; Guo, Z.; Liu, H.; Ouyang, L.; Zhu, M.; Yu, X. Monodisperse magnesium hydride nanoparticles uniformly self-assembled on graphene. *Adv. Mater.* **2015**, *27*, 5981−5988.

(7) Ali, W.; Luo, M.; Wu, M.; Saddique, J.; Bai, Y.; Ding, S.; Wu, C.; Hu, W. Bimetal Three-Dimensional MXene Nanostructures Stabilizing Magnesium Hydrides Realize Long Cyclic Life and Faster Kinetic Rates. *ACS Sustainable Chem. Eng.* **2023**, *11*, 17157−17167.

(8) Ali, W.; Li, X.; Yang, Y.; Li, N.; Huang, B.; Wu, C.; Ding, S. In Situ Formed Ti/Nb Nanocatalysts within a Bimetal 3D MXene Nanostructure Realizing Long Cyclic Lifetime and Faster Kinetic Rates of MgH2. *ACS Appl. Mater. Interfaces* **2023**, *15*, 36167−36178.

(9) Zou, R.; Adedeji Bolarin, J.; Lei, G.; Gao, W.; Li, Z.; Cao, H.; Chen, P. Microwave-assisted reduction of Ti species in MgH2-TiO2 composite and its effect on hydrogen storage. *Chem. Eng. J.* **2022**, *450*, 138072.

(10) Wen, X.; Liang, H.; Zhao, R.; Hong, F.; Shi, W.; Liu, H.; Chen, H.; Zhou, W.; Guo, J.; Lan, Z. Regulation of the integrated hydrogen storage properties of magnesium hydride using 3D self-assembled amorphous carbon-embedded porous niobium pentoxide. *J. Mater. Chem. A* **2022**, *10*, 16941−16951.

(11) Pukazhselvan, D.; Reis Silva, D. A.; Sandhya, K. S.; Fateixa, S.; Shaula, A.; Nogueira, H.; Bdikin, I.; Fagg, D. P. Interaction of zirconia with magnesium hydride and its influence on the hydrogen storage behavior of magnesium hydride. *Int. J. Hydrogen Energy* **2022**, *47*, 21760−21771.

(12) Chen, J.; Xia, G.; Guo, Z.; Huang, Z.; Liu, H.; Yu, X. Porous Ni nanofibers with enhanced catalytic effect on the hydrogen storage performance of MgH2. *J. Mater. Chem. A* **2015**, *3*, 15843−15848.

(13) Dan, L.; Wang, H.; Liu, J.; Ouyang, L.; Zhu, M. H2 Plasma Reducing Ni Nanoparticles for Superior Catalysis on Hydrogen Sorption of MgH2. *ACS Appl. Energy Mater.* **2022**, *5*, 4976−4984.

(14) Xia, G.; Tan, Y.; Chen, X.; Sun, D.; Guo, Z.; Liu, H.; Ouyang, L.; Zhu, M.; Yu, X. Monodisperse Magnesium Hydride Nanoparticles Uniformly Self-Assembled on Graphene. *Adv. Mater.* **2015**, *27*, 5981−5988.

(15) Meng, Q.; Huang, Y.; Ye, J.; Xia, G.; Wang, G.; Dong, L.; Yang, Z.; Yu, X. Electrospun carbon nanofibers with in-situ encapsulated Ni nanoparticles as catalyst for enhanced hydrogen storage of MgH2. *J. Alloys Compd.* **2021**, *851*, 156874.

(16) Yao, P.; Jiang, Y.; Liu, Y.; Wu, C.; Chou, K.-C.; Lyu, T.; Li, Q. Catalytic effect of Ni@rGO on the hydrogen storage properties of MgH2. *J. Magnesium Alloys* **2020**, *8*, 461−471.
(17) Ma, Z.; Tang, Q.; Ni, J.; Zhu, Y.; Zhang, Y.; Li, H.-W.; Zhang, J.; Liu, Y.; Ba, Z.; Li, L. Synergistic effect of TiH2 and air exposure on enhancing hydrogen storage performance of Mg2NiH4. *Chem. Eng. J.* **2022**, *433*, 134489.
(18) Gao, H.; Shi, R.; Shao, Y.; Liu, Y.; Zhu, Y.; Zhang, J.; Li, L. Catalysis derived from flower-like Ni MOF towards the hydrogen storage performance of magnesium hydride. *Int. J. Hydrogen Energy* **2022**, *47*, 9346−9356.
(19) Ma, Z.; Zhang, J.; Zhu, Y.; Lin, H.; Liu, Y.; Zhang, Y.; Zhu, D.; Li, L. Facile Synthesis of Carbon Supported Nano-Ni Particles with Superior Catalytic Effect on Hydrogen Storage Kinetics of MgH2. *ACS Appl. Energy Mater.* **2018**, *1*, 1158−1165.
(20) Zhu, W.; Panda, S.; Lu, C.; Ma, Z.; Khan, D.; Dong, J.; Sun, F.; Xu, H.; Zhang, Q.; Zou, J. Using a Self-Assembled Two-Dimensional MXene-Based Catalyst (2D-Ni@Ti3C2) to Enhance Hydrogen Storage Properties of MgH2. *ACS Appl. Mater. Interfaces* **2020**, *12*, 50333−50343.
(21) Gao, H.; Shao, Y.; Shi, R.; Liu, Y.; Zhu, J.; Liu, J.; Zhu, Y.; Zhang, J.; Li, L.; Hu, X. Effect of Few-Layer $Ti_3C_2T_{<i>x</i>}$ Supported Nano-Ni via Self-Assembly Reduction on Hydrogen Storage Performance of MgH_2. *ACS Appl. Mater. Interfaces* **2020**, *12*, 47684−47694.
(22) Peng, C.; Yang, C.; Zhang, Q. Few-layer MXene $Ti_3C_2T_{<i>x</i>}$ supported Ni@C nanoflakes as a catalyst for hydrogen desorption of MgH_2. *J. Mater. Chem. A* **2022**, *10*, 12409−12417.
(23) Jeong, U.; Kim, H.; Ramesh, S.; Dogan, N. A.; Wongwilawan, S.; Kang, S.; Park, J.; Cho, E. S.; Yavuz, C. T. Rapid Access to Ordered Mesoporous Carbons for Chemical Hydrogen Storage. *Angew. Chem., Int. Ed.* **2021**, *60*, 22478−22486.
(24) Cho, Y.; Kang, S.; Wood, B. C.; Cho, E. S. Heteroatom-Doped Graphenes as Actively Interacting 2D Encapsulation Media for Mg-Based Hydrogen Storage. *ACS Appl. Mater. Interfaces* **2022**, *14*, 20823−20834.
(25) Wan, L. F.; Cho, E. S.; Marangoni, T.; Shea, P.; Kang, S.; Rogers, C.; Zaia, E.; Cloke, R. R.; Wood, B. C.; Fischer, F. R.; Urban, J. J.; Prendergast, D. Edge-Functionalized Graphene Nanoribbon Encapsulation To Enhance Stability and Control Kinetics of Hydrogen Storage Materials. *Chem. Mater.* **2019**, *31*, 2960−2970.
(26) Cui, H.; Tian, W.; Zhang, Y.; Liu, T.; Wang, Y.; Shan, P.; Chen, Y.; Yuan, H. Study on the hydrogen storage performance of graphene(N)-Sc-graphene(N) structure. *Int. J. Hydrogen Energy* **2020**, *45*, 33789−33797.
(27) Khan, Z. U.; Yan, T.; Shi, L.; Zhang, D. Improved capacitive deionization by using 3D intercalated graphene sheet-sphere nanocomposite architectures. *Environ. Sci.: Nano* **2018**, *5*, 980−991.
(28) Guemou, S.; Zhang, L.; Li, S.; Jiang, Y.; Zhong, T.; Lu, Z.; Zhou, R.; Wu, F.; Li, Q. Exceptional catalytic effect of novel rGO-supported Ni-Nb nanocomposite on the hydrogen storage properties of MgH2. *J. Mater. Sci. Technol.* **2024**, *172*, 83−93.
(29) Ding, S.; Qiao, Y.; Cai, X.; Du, C.; Wen, Y.; Shen, X.; Xu, L.; Guo, S.; Gao, W.; Shen, T. Catalytic mechanisms of nickel nanoparticles for the improved dehydriding kinetics of magnesium hydride. *J. Magnesium Alloys* **2023**.
(30) Yu, Z.; Liu, X.; Liu, Y.; Li, Y.; Zhang, Z.; Chen, K.; Han, S. Synergetic catalysis of Ni@C@CeO2 for driving ab/desorption of MgH2 at moderate temperature. *Fuel* **2024**, *357*, 129726.
(31) Jia, Z.; Zhao, B.; Zhao, Y.; Liu, B.; Yuan, J.; Zhang, J.; Zhu, Y.; Wu, Y.; Li, L. Boron nitride supported nickel nanoparticles as catalyst for enhancing the hydrogen storage properties of MgH2. *J. Alloys Compd.* **2022**, *927*, 166853.
(32) Tome, K. C.; Xi, S.; Fu, Y.; Lu, C.; Lu, N.; Guan, M.; Zhou, S.; Yu, H. Remarkable catalytic effect of Ni and ZrO2 nanoparticles on the hydrogen sorption properties of MgH2. *Int. J. Hydrogen Energy* **2022**, *47*, 4716−4724.
(33) Yao, P.; Jiang, Y.; Liu, Y.; Wu, C.; Chou, K.-C.; Lyu, T.; Li, Q. Catalytic effect of Ni@rGO on the hydrogen storage properties of MgH2. *J. Magnesium Alloys* **2020**, *8*, 461−471.
(34) Zeng, L.; Lan, Z.; Li, B.; Liang, H.; Wen, X.; Huang, X.; Tan, J.; Liu, H.; Zhou, W.; Guo, J. Facile synthesis of a Ni3S2@C composite using cation exchange resin as an efficient catalyst to improve the kinetic properties of MgH2. *J. Magnesium Alloys* **2022**, *10*, 3628−3640.
(35) Li, L.; Zhang, Z.; Jiao, L.; Yuan, H.; Wang, Y. In situ preparation of nanocrystalline Ni@C and its effect on hydrogen storage properties of MgH2. *Int. J. Hydrogen Energy* **2016**, *41*, 18121−18129.
(36) Xia, G.; Tan, Y.; Chen, X.; Sun, D.; Guo, Z.; Liu, H.; Ouyang, L.; Zhu, M.; Yu, X. Monodisperse Magnesium Hydride Nanoparticles Uniformly Self Assembled on Graphene. *Adv. Mater.* **2015**, *27*, 5981−5988.
(37) Ali, W.; Qin, Y.; Khan, N. A.; Zhao, H.; Su, Y.; Ding, D.; Huang, B.; Wu, C.; Hu, W.; Ding, S. Highly air-stable magnesium hydrides encapsulated by nitrogen-doped graphene nanospheres with favorable hydrogen storage kinetics. *Chem. Eng. J.* **2024**, *480*, 148163.
(38) Cho, Y.; Kang, S.; Wood, B. C.; Cho, E. S. Heteroatom-Doped Graphenes as Actively Interacting 2D Encapsulation Media for Mg-Based Hydrogen Storage. *ACS Appl. Mater. Interfaces* **2022**, *14*, 20823−20834.

https://doi.org/10.1021/acsomega.4c00198
ACS Omega 2024, 9, 19261−19271